



Available online at [www.sciencedirect.com](http://www.sciencedirect.com)



Franklin Institute 00 (2023) 1–20

Franklin  
Institute

# Linear Quadratic Integral Differential Game applied to the Real-time Control of a Quadrotor Experimental setup

Hadi Nobahari

*Department of Aerospace Engineering Sharif University of Technology Tehran, Iran*

Ali BaniAsad

*Department of Aerospace Engineering Sharif University of Technology Tehran, Iran*

Reza Pordal

*Department of Aerospace Engineering Sharif University of Technology Tehran, Iran*

Alireza Sharifi

*Department of Aerospace Engineering Sharif University of Technology Tehran, Iran*

---

## Abstract

This research paper introduces a novel approach to attitude control for quadrotors, employing a linear quadratic Gaussian (LQG) controller with integral actions based on differential game theory. Accurate attitude control is of utmost importance for safe and effective quadrotor flight, particularly in the presence of disturbances. To develop a reliable and efficient control system, the nonlinear equations of motion for the quadrotor's experimental setup are linearized to derive a continuous state-space model. The model parameters are identified through experimental data, and a two-player approach is employed to determine the attitude control commands. One player optimizes the command while the other creates disturbances by mini-maximizing a quadratic criterion, defined as the sum of outputs and disturbances weighted by control effort. The performance of the proposed approach is evaluated by comparing it to a linear quadratic regulator controller in level flight. The results demonstrate that the proposed approach effectively dissipates disturbances and outperforms linear quadratic regulator controllers, thereby contributing to the development of robust and effective attitude control systems for quadrotors.

© 2011 Published by Elsevier Ltd.

**Keywords:**

Linear quadratic Gaussian controller, Differential game theory, Quadrotor, Continuous state-space model, 3-axis experimental setup, Optimal attitude control, Robust disturbance rejection.

---

## 1. Introduction

Research, military, imaging, recreation, and agriculture are all used by quadrotors in today's society [1]. Various subsystems of the quadrotor control system are responsible for the quadrotor's performance, including attitude,

---

*Email addresses:* nobahari@sharif.edu (Hadi Nobahari), ali.baniasad@ae.sharif.edu (Ali BaniAsad), email address (Reza Pordal), alireza\_sharifi@ae.sharif.edu (Alireza Sharifi)

altitude, and position. Quadrotor attitude control requires maintaining the desired attitude outputs by controlling the rotational speed of the rotors[2], for example, in the event of sudden disturbances. Due to this, much research is being conducted on automatically controlling the quadrotors that control the attitude when they encounter disturbances. The quadrotor attitude is controlled by a Proportional Integral Derivative (PID) controller in [3, 4]. During disturbances, however, this controller has not effectively achieved the control objectives. Model-based approaches to controller design are utilized to resolve this issue [5, 6]. Quadrotor attitude models and disturbances determine the direction of the best control commands using these controllers.

The literature has proposed numerous models-based controllers to provide a faster control algorithm when dealing with modeling errors and reducing disturbances. An intelligent controller, a robust controller, a nonlinear controller, and an optimal controller are some of these types of controllers.

Control approaches based on intelligent logic, machine learning [7], iterative learning[8], such as fuzzy logic[9], reinforcement learning [10], and evolutionary computation [11] have been widely utilized to regulate the attitude of quadrotors.

Several nonlinear control techniques have been proposed to control the roll, pitch, and yaw angles of quadrotors, including Synergetic Control [12], Sliding Mode Control (SMC) [13], and Feedback Linearization (FBL) [14]. Robust control methods such as  $H_{\infty}$  [15, 16] and  $\mu$ -synthesis [17] have also been utilized to stabilize the attitudes of quadrotors under conditions of extreme uncertainty and worst-case scenarios. Optimal controllers, including the Linear Quadratic Regulator (LQR) [18] and Linear Quadratic Gaussian (LQG) [19], have also been employed in controlling quadrotors. A quadratic criterion is minimized when the controllers provide optimal feedback gains by taking into account both regulation performance and control effort. The Linear Quadratic Regulator Differential Game (LQR-DG) control approach [20, 21] is an optimal and robust control technique that utilizes a linear model of a system to control its outputs while minimizing a cost function through mini-maximization. This approach has been applied to control various nonlinear and complex systems, including a ship controller [22, 23]. Through an analytical pursuit-evasion process, the LQR-DG control method generates control commands. This approach sets the LQR-DG controller apart from other optimal control methods and allows one player to track the best control command while the other creates disturbances.

This study proposes a new controller for quadrotors based on the LQG technique with integral action, using differential game theory to optimize control performance in the presence of disturbance. Attitude control in the presence of disturbance is essential for ensuring safe and effective quadrotor flight. To develop this control approach, a continuous state-space model for a quadrotor's experimental setup is derived through linearization of the system's nonlinear equations of motion, and its parameters are identified using experimental data. The proposed LQIG-DG controller generates the most efficient control commands for the quadrotor, with a two-player approach where one player optimizes the command and the other creates disturbances by mini-maximizing a quadratic criterion. The proposed approach is evaluated against a linear quadratic regulator controller in level flight. The results show that the LQIG-DG controller effectively dissipates disturbances and outperforms the linear quadratic regulator controller. This study presents an important contribution to the development of robust and effective attitude control systems for quadrotors.

In the following sections of this paper, the problem is defined in section 2. The dynamics model and the estimation problem for the experimental setup of the quadrotor are derived in detail in sections 3, respectively. In section 4, the proposed LQIG-DG controller architecture is explained. The effectiveness of the controller is then evaluated in section 5, followed by the conclusion in section 6.

## 2. Problem Statement

A nonlinear dynamic describes the experimental setup of the quadrotor in Figure 1. During its rotation, the quadrotor can adjust its pitch, roll, and yaw angles. An Inertial Measurement Unit (IMU) is used to measure the acceleration and angular velocities along the three orthogonal axes, which are affected by noise. To estimate the quadrotor states, including the Euler angles and angular velocities, a nonlinear filter is employed. A block diagram of the LQIG-DG controller structure is illustrated in Figure 2. Because of the estimated states, the quadrotor setup can be stabilized.



Figure 1: 3DoF setup of the quadrotor.

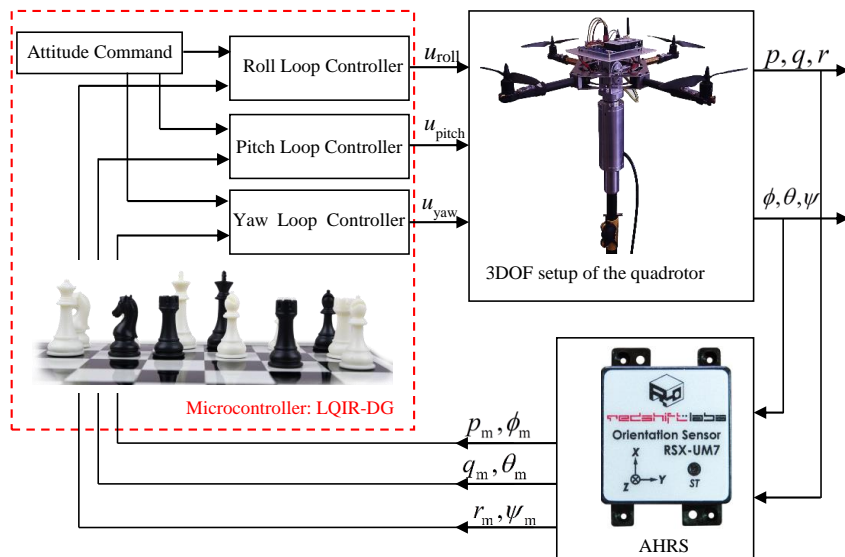


Figure 2: Block diagram of the LQIG-DG controller structure.

### 3. Nonlinear Dynamic Model for the Quadrotor Setup

An analysis of the quadrotor's three degrees of freedom is presented here, followed by a nonlinear model for the attitude dynamics in state-space form. A linearization of the nonlinear model is completed in order to use it as a LQIR-DG control model.

#### 3.1. Quadrotor Configuration and Attitude Dynamics Model

The schematic of the quadrotor is depicted in Figure 3, showing each rotor with an angular velocity,  $\Omega_r$ , rotating around the  $z_B$  axis in the body coordinate system. The counterclockwise rotation of Rotor 1 and Rotor 3 counteracts the yawing moment, while the clockwise rotation of Rotors 2 and 4 counteracts the yawing moment.

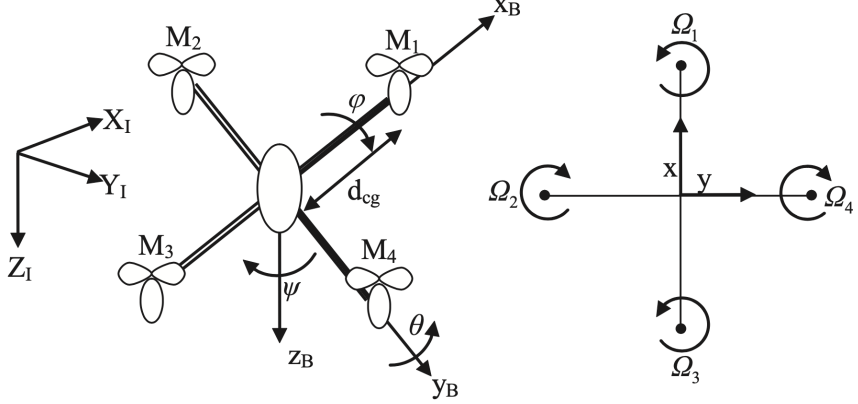


Figure 3: Configuration of the quadrotor.

### 3.2. Dynamic Modeling of the Quadrotor Setup

The dynamic model of the quadrotor setup is an essential component for control design. In this section, the quadrotor dynamic model is derived using the Newton-Euler method [24, 25].

$$\dot{p} = \frac{I_{yy} - I_{zz}}{I_{xx}} qr + q \frac{I_{rotor}}{I_{xx}} \Omega_r + \frac{u_{roll}}{I_{xx}} + \frac{d_{roll}}{I_{xx}} \quad (1)$$

$$\dot{q} = \frac{I_{zz} - I_{xx}}{I_{yy}} rp + p \frac{I_{rotor}}{I_{xx}} \Omega_r + \frac{u_{pitch}}{I_{yy}} + \frac{d_{pitch}}{I_{yy}} \quad (2)$$

$$\dot{r} = \frac{I_{xx} - I_{yy}}{I_{zz}} pq + \frac{u_{yaw}}{I_{zz}} + \frac{d_{yaw}}{I_{zz}} \quad (3)$$

The variables  $(p, q, r)$  represent the angular velocities, while the variables  $d_{roll}$ ,  $d_{pitch}$ , and  $d_{yaw}$  denote the disturbances produced in  $x_B$ ,  $y_B$ , and  $z_B$ , respectively. Additionally,  $I_{xx}$ ,  $I_{yy}$ , and  $I_{zz}$  are the principal moments of inertia, and  $I_{rotor}$  is the rotor inertia about its axis. Euler angle rates are also determined from angular body rates:

$$\begin{bmatrix} \dot{\phi} \\ \dot{\theta} \\ \dot{\psi} \end{bmatrix} \begin{bmatrix} 1 & \sin(\phi) \tan(\theta) & \cos(\phi) \tan(\theta) \\ 0 & \cos(\phi) & -\sin(\phi) \\ 0 & \sin(\phi)/\cos(\theta) & \cos(\phi)/\cos(\theta) \end{bmatrix} \begin{bmatrix} p \\ q \\ r \end{bmatrix} \quad (4)$$

The quadrotor system has three degrees of freedom: roll, pitch, and yaw. The rotational motion is described by the angles  $(\phi, \theta, \psi)$ , which represent roll, pitch, and yaw, respectively. The overall residual rotor angular velocity, denoted by  $\Omega_r$ , is calculated as follows:

$$\Omega_r = -\Omega_1 + \Omega_2 - \Omega_3 + \Omega_4 \quad (5)$$

### 3.3. Innovative Control Strategies for Quadrotor

The control inputs  $u_{roll}$ ,  $u_{pitch}$ , and  $u_{yaw}$  are roll, pitch, and yaw moments, generated by the quadrotor's rotors, and defined as follows:

$$u_{roll} = b d_{cg} (\Omega_2^2 - \Omega_4^2) \quad (6)$$

$$u_{pitch} = b d_{cg} (\Omega_1^2 - \Omega_3^2) \quad (7)$$

$$u_{yaw} = d (\Omega_1^2 - \Omega_2^2 + \Omega_3^2 - \Omega_4^2) \quad (8)$$

The quadrotor's drag and thrust coefficients are denoted by  $d$  and  $b$ , respectively. The distance between the rotors and the gravity center is represented by  $d_{cg}$ . The angular velocity commands can be computed as follows:

$$\Omega_{c,1}^2 = \Omega_{\text{mean}}^2 + \frac{1}{2b d_{cg}} u_{\text{pitch}} + \frac{1}{4d} u_{\text{yaw}} \quad (9)$$

$$\Omega_{c,2}^2 = \Omega_{\text{mean}}^2 + \frac{1}{2b d_{cg}} u_{\text{roll}} - \frac{1}{4d} u_{\text{yaw}} \quad (10)$$

$$\Omega_{c,3}^2 = \Omega_{\text{mean}}^2 - \frac{1}{2b d_{cg}} u_{\text{pitch}} + \frac{1}{4d} u_{\text{yaw}} \quad (11)$$

$$\Omega_{c,4}^2 = \Omega_{\text{mean}}^2 - \frac{1}{2b d_{cg}} u_{\text{roll}} - \frac{1}{4d} u_{\text{yaw}} \quad (12)$$

The nominal angular velocities of the rotors are denoted by  $\Omega_{\text{mean}}$ .

### 3.4. State-Space Representation of Quadrotor Dynamics

The formulation of a state-space model is crucial for the development of advanced control strategies. In this context, a state-space representation of the quadrotor system is provided in order to facilitate the design of control algorithms.

In order for the quadrotor to be controlled, it can be modelled in state-space by introducing the following variables:  $x_1 = p$ ,  $x_2 = q$ ,  $x_3 = r$ ,  $x_4 = \phi$ ,  $x_5 = \theta$ , and  $x_6 = \psi$ .

$$\dot{x}_1 = \Gamma_1 x_2 x_3 + \Gamma_2 x_2 \Omega_r + \Gamma_3 u_{\text{roll}} + \Gamma_3 d_{\text{roll}} \quad (13)$$

$$\dot{x}_2 = \Gamma_4 x_1 x_3 - \Gamma_5 x_1 \Omega_r + \Gamma_6 u_{\text{pitch}} + \Gamma_6 d_{\text{pitch}} \quad (14)$$

$$\dot{x}_3 = \Gamma_7 x_1 x_2 + \Gamma_8 u_{\text{yaw}} + \Gamma_8 d_{\text{yaw}} \quad (15)$$

$$\dot{x}_4 = x_1 + (x_2 \sin(x_4) + x_3 \cos(x_4)) \tan(x_5) \quad (16)$$

$$\dot{x}_5 = x_2 \cos(x_4) - x_3 \sin(x_4) \quad (17)$$

$$\dot{x}_6 = (x_2 \sin(x_4) + x_3 \cos(x_4)) / \cos(x_5) \quad (18)$$

Furthermore, to facilitate the analysis,  $\Gamma_i (i = 1, \dots, 8)$  is introduced, which represents a set of coefficients related to the quadrotor's physical properties and external factors.

$$\begin{aligned} \Gamma_1 &= \frac{I_{yy} - I_{zz}}{I_{xx}}, & \Gamma_2 &= \frac{I_{\text{rotor}}}{I_{xx}}, & \Gamma_3 &= \frac{1}{I_{xx}} \\ \Gamma_4 &= \frac{I_{zz} - I_{xx}}{I_{yy}}, & \Gamma_5 &= \frac{I_{\text{rotor}}}{I_{xx}}, & \Gamma_6 &= \frac{1}{I_{yy}} \\ \Gamma_7 &= \frac{I_{xx} - I_{yy}}{I_{zz}}, & \Gamma_8 &= \frac{1}{I_{zz}} \end{aligned} \quad (19)$$

For the purpose of control, the measurement model can be expressed as follows:

$$\mathbf{z} = [p_m \quad q_m \quad r_m \quad \phi_m \quad \theta_m \quad \psi_m]^T \quad (20)$$

### 3.5. Linearization of the Nonlinear Quadrotor Model

The use of a continuous-time linear model allows for the effective control of the quadrotor. The linear state-space model is denoted as follows:

$$\dot{\mathbf{x}}(t) = \mathbf{A} \mathbf{x}(t) + \mathbf{B} \mathbf{u}(t) + \mathbf{B}_d \mathbf{d}(t) \quad (21)$$

The system, input, and disturbance matrices are denoted by  $\mathbf{A}$ ,  $\mathbf{B}$ , and  $\mathbf{B}_d$ , respectively, with  $\mathbf{d}$  representing the disturbance. The measurement equation is given by

$$\mathbf{z}(t) = \mathbf{x}(t) \quad (22)$$

In light of the differential equations given by Equations (13)-(18), the linear dynamic model corresponding to the equilibrium points ( $\mathbf{x}_e=0$  and  $\mathbf{u}_e=0$ ) of the quadrotor setup can be expressed as follows:

$$\begin{aligned} \dot{\mathbf{x}} = & \begin{bmatrix} \dot{\mathbf{x}}_{\text{roll}} \\ \dot{\mathbf{x}}_{\text{pitch}} \\ \dot{\mathbf{x}}_{\text{yaw}} \end{bmatrix} = \begin{bmatrix} \mathbf{A}_{\text{roll}} & \mathbf{0} & \mathbf{0} \\ \mathbf{0} & \mathbf{A}_{\text{pitch}} & \mathbf{0} \\ \mathbf{0} & \mathbf{0} & \mathbf{A}_{\text{yaw}} \end{bmatrix} \begin{bmatrix} \mathbf{x}_{\text{roll}} \\ \mathbf{x}_{\text{pitch}} \\ \mathbf{x}_{\text{yaw}} \end{bmatrix} \\ & + \begin{bmatrix} \mathbf{B}_{\text{roll}} & \mathbf{0} & \mathbf{0} \\ \mathbf{0} & \mathbf{B}_{\text{pitch}} & \mathbf{0} \\ \mathbf{0} & \mathbf{0} & \mathbf{B}_{\text{yaw}} \end{bmatrix} \begin{bmatrix} \mathbf{u}_{\text{roll}} \\ \mathbf{u}_{\text{pitch}} \\ \mathbf{u}_{\text{yaw}} \end{bmatrix} \\ & + \begin{bmatrix} \mathbf{B}_{\text{roll}} & \mathbf{0} & \mathbf{0} \\ \mathbf{0} & \mathbf{B}_{\text{pitch}} & \mathbf{0} \\ \mathbf{0} & \mathbf{0} & \mathbf{B}_{\text{yaw}} \end{bmatrix} \begin{bmatrix} \mathbf{d}_{\text{roll}} \\ \mathbf{d}_{\text{pitch}} \\ \mathbf{d}_{\text{yaw}} \end{bmatrix} \end{aligned} \quad (23)$$

where  $\mathbf{x}_{\text{roll}} = [p \ \phi]^T$ ,  $\mathbf{x}_{\text{pitch}} = [q \ \theta]^T$ , and  $\mathbf{x}_{\text{yaw}} = [r \ \psi]^T$ .

Moreover, the state and input matrices are presented as

$$\mathbf{A}_{\text{roll}} = \mathbf{A}_{\text{pitch}} = \mathbf{A}_{\text{yaw}} = \begin{bmatrix} 0 & 0 \\ 1 & 0 \end{bmatrix} \quad (24)$$

$$\mathbf{B}_{\text{roll}} = \begin{bmatrix} 1 \\ I_{xx} \\ 0 \end{bmatrix}; \quad \mathbf{B}_{\text{pitch}} = \begin{bmatrix} 1 \\ I_{yy} \\ 0 \end{bmatrix}; \quad \mathbf{B}_{\text{yaw}} = \begin{bmatrix} 1 \\ I_{zz} \\ 0 \end{bmatrix} \quad (25)$$

### 3.6. Identification of the Setup Parameters

This section presents an optimization technique for estimating the model parameters ( $\Gamma$ ) of the 3DOF experimental setup from experimental data. The technique is based on the Nonlinear Least Squares (NLS) method, which is widely used in parameter estimation problems. The NLS algorithm utilizes the trust-region reflective least squares (TRRLS) method to iteratively find the values of the model parameters. The goal is to minimize a cost function, which is based on the sum of squares between the input/output signals provided by the simulation model and the experimental ones.

The optimization process involves finding a vector  $\mathbf{\Gamma}$  that minimizes the cost function. This is achieved by iteratively updating the values of the model parameters until convergence is achieved. The NLS method is particularly useful for problems where the model is nonlinear and the measurement noise is known. The approach is based on a least squares problem, where the objective is to find the values of  $\mathbf{\Gamma}$  that minimize the sum of squares function [26]:

$$\min_{\Gamma_i} (\| e(\Gamma_i) \|^2) = \min_{\Gamma_i} = \left( \sum_{i=1}^n (y - \hat{y})^2 \right) \quad (26)$$

where  $y$  and  $\hat{y}$  are the experimental and simulated output signals, when the same input signals are applied ones. The structure of the proposed identification approach is illustrated in Figure 4.

In summary, the NLS optimization technique is an effective approach for estimating the model parameters of the 3DOF experimental setup from experimental data. The technique utilizes the TRRLS method to iteratively update the values of the model parameters, with the goal of minimizing the difference between the simulation model and the experimental data.

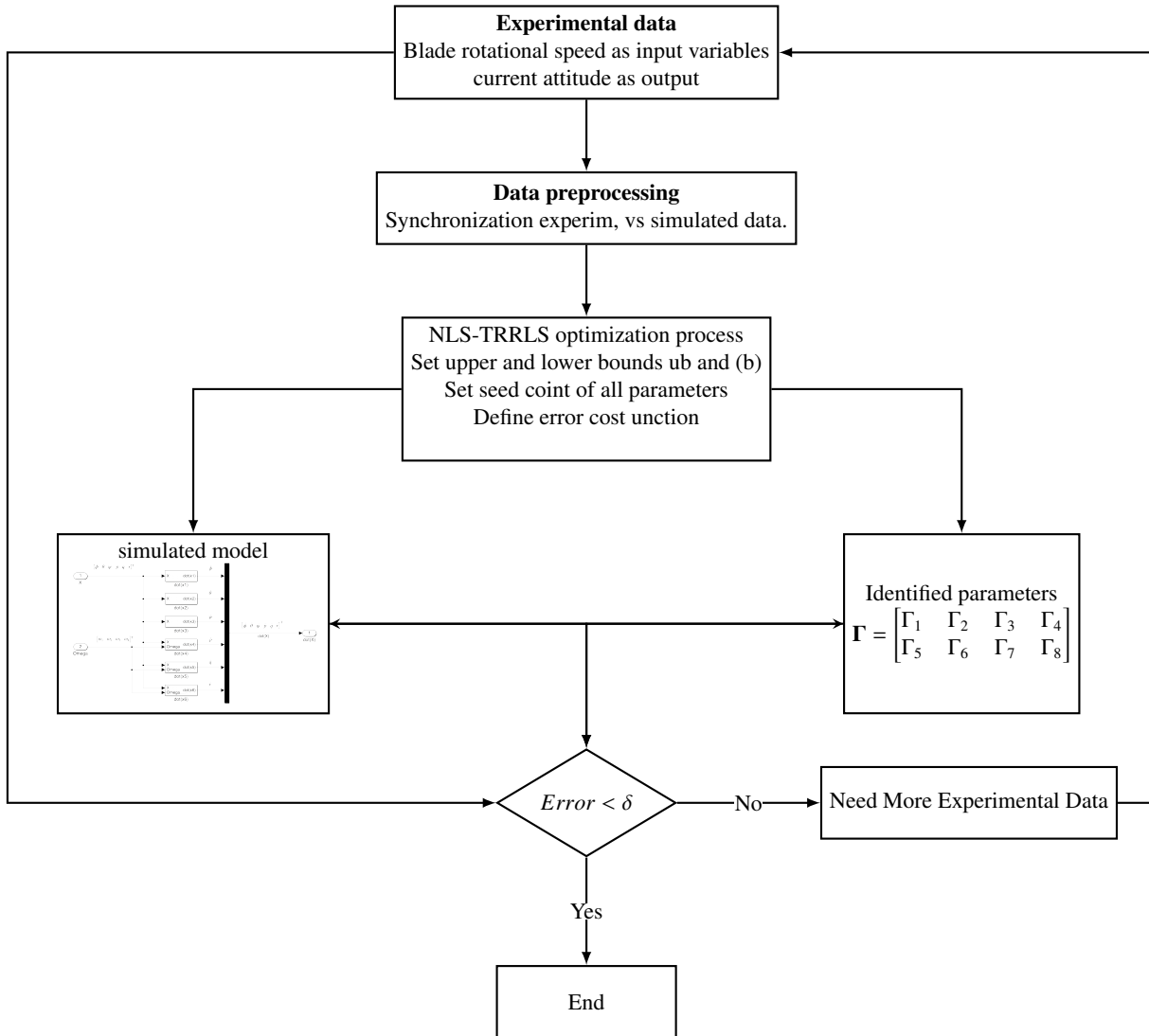


Figure 4: Structure of TRRLS identification approach.

#### 4. Formulation of the Controller Design

In the LQIR-DG controller structure, an integral action is added to the LQR-DG controller to cancel the steady-state errors for reference tracking. For this purpose, first, the augmented state space of the linear quadrotor model is defined to utilize in the controller architecture. Then, the LQR-DG controller design procedure is presented to produce the best control commands for the experimental setup of the quadrotor.

##### 4.1. Augmented State Space Formulation

To add the integral action to the controller structure, the augmented states are defined as follows:

$$\mathbf{x}_{\text{ai}} = \begin{bmatrix} \mathbf{x}_i & \int \mathbf{x}_i \end{bmatrix}^T \quad (27)$$

where  $i = \text{roll, pitch, and yaw}$ . Then, the quadrotor dynamics model, denoted by Eq.(21), is denoted in the augmented state-space model as

$$\dot{\mathbf{x}}_a(t) = \mathbf{A}_a \mathbf{x}_a(t) + \mathbf{B}_a \mathbf{u}(t) + \mathbf{B}_{d_a} \mathbf{d}(t) \quad (28)$$

where matrices  $\mathbf{A}_a$  and  $\mathbf{B}_a$  are defined as follows:

$$\mathbf{A}_a = \begin{bmatrix} \mathbf{A} & \mathbf{0} \\ \mathbf{I} & \mathbf{0} \end{bmatrix} \quad (29)$$

$$\mathbf{B}_a = \mathbf{B}_{d_a} = \begin{bmatrix} \mathbf{B} \\ \mathbf{0} \end{bmatrix} \quad (30)$$

In the above equation  $\mathbf{I}$  denotes the identity matrix.

#### 4.2. LQIR-DG Controller Method

The LQIR-DG controller is an optimal and robust method based on the differential game theory. This controller consists of two essential players: one finds the best control command, and the other creates the worst disturbance. For this purpose, the first player tries to minimize a cost function, while the second is assumed to maximize it. Therefore, the quadratic cost function equation is denoted using min-max operators as follows:

$$\min_u \max_d J(\mathbf{x}_{a_i}, u_i, d_i) = J(\mathbf{x}_{a_i}, u_i^*, d_i^*) = \min_u \max_d \int_0^{t_f} \left( \mathbf{x}_{a_i}^T \mathbf{Q}_i \mathbf{x}_{a_i} + u_i^T R u_i - d_i^T R_d d_i \right) dt \quad (31)$$

where  $R$  and  $R_d$  are symmetric nonnegative definite matrices and  $\mathbf{Q}_i$  is a symmetric positive definite matrix. Moreover,  $t_f$  is the final time. ??????????????????To solve this problem, connections between the general optimal problem and the LQIR problem are considered [20]. Consequently, the optimum control effort is computed for each control loop as follows:

$$u_i(t) = -\mathbf{K}_i(t) \mathbf{x}_{a_i}(t) \quad (32)$$

$$d_i(t) = \mathbf{K}_{d_i}(t) \mathbf{x}_{a_i}(t) \quad (33)$$

where  $\mathbf{K}_i$  and  $\mathbf{K}_{d_i}$  are a time varying gain, given by

$$\mathbf{K}_i = R^{-1} \mathbf{B}_{a_i}^T \mathbf{P}_{a_i}(t) \quad (34)$$

$$\mathbf{K}_{d_i} = R_d^{-1} \mathbf{B}_{d_i}^T \mathbf{P}_{d_i}(t) \quad (35)$$

where  $\mathbf{P}_{a_i}(t)$  and  $\mathbf{P}_{d_i}(t)$  satisfy

$$\dot{\mathbf{P}}_{a_i}(t) = -\mathbf{A}_a^T \mathbf{P}_{a_i}(t) - \mathbf{P}_{a_i}(t) \mathbf{A}_a - \mathbf{Q}_i + \mathbf{P}_{a_i}(t) \mathbf{S}_{a_i}(t) \mathbf{P}_{a_i}(t) + \mathbf{P}_{a_i}(t) \mathbf{S}_{a_{d_i}}(t) \mathbf{P}_{a_{d_i}}(t) \quad (36)$$

$$\dot{\mathbf{P}}_{d_i}(t) = -\mathbf{A}_a^T \mathbf{P}_{d_i}(t) - \mathbf{P}_{d_i}(t) \mathbf{A}_a - \mathbf{Q}_i + \mathbf{P}_{d_i}(t) \mathbf{S}_{d_i}(t) \mathbf{P}_{d_i}(t) + \mathbf{P}_{d_i}(t) \mathbf{S}_{a_i}(t) \mathbf{P}_{a_i}(t) \quad (37)$$

where  $\mathbf{S}_{a_i} = \mathbf{B}_{a_i} R^{-1} \mathbf{B}_{a_i}^T$  and  $\mathbf{S}_{a_{d_i}} = \mathbf{B}_{d_i} R_d^{-1} \mathbf{B}_{d_i}^T$ . In this study, the steady-state values of the above equations ( $\mathbf{P}$  as  $t_f \rightarrow \infty$ ) are utilized to generate a feedback control law.

## 5. Result and Discussion

Here, the results of the LQIR-DG controller method are devoted to the control loops of the roll, pitch, and yaw of the experimental setup of the quadrotor. First, the controller parameters are tuned using the results of numerical simulations. Moreover, the performance of the LQIR-DG controller is compared to an LQR control strategy. The quadrotor parameters are shown in table 1. Moreover, the parameters of LQIR-DG controller weight are denoted in table 2.

Table 1: The Parameter of the Quadrotor

Parameter	Value	Unit
$I_{xx}$	0.02839	$\text{kg} \cdot \text{m}^2$
$I_{yy}$	0.03066	$\text{kg} \cdot \text{m}^2$
$I_{zz}$	0.0439	$\text{kg} \cdot \text{m}^2$
$I_{\text{rotor}}$	$4.4398 \times 10^{-5}$	$\text{kg} \cdot \text{m}^2$
$b$	$3.13 \times 10^{-5}$	$\text{N} \cdot \text{sec}^2 / \text{rad}^2$
$d$	$3.2 \times 10^{-6}$	$\text{N} \cdot \text{m} \cdot \text{sec}^2 / \text{rad}^2$
$\Omega_{\text{mean}}$	3000	rpm
$d_{cg}$	0.2	m

Table 2: The Parameters of the LQIR-DG Controller

Control Loop	Weight	Value
Roll	$\mathbf{Q}_{\text{roll}}$	$\text{diag}([0.02, 65.96, 83.04, 0.00])$
Pitch	$\mathbf{Q}_{\text{pitch}}$	$\text{diag}([435.01, 262.60, 262.60, 0.00])$
Yaw	$\mathbf{Q}_{\text{yaw}}$	$\text{diag}([4e-4, 0.00, 0.133, 0])$
-	$R$	1
-	$R_d$	1.2764

### 5.1. Identification of the 3DoF experimental setup model

As denoted in section 3.4, the parameters of the quadrotor setup are  $\Gamma_i (i = 1, \dots, 8)$  that need to be identified based on the NRS algorithm. The NLS-TRRLS algorithm is performed in the Matlab R2022b®. In order to increase accuracy identification of parameters, three scenarios, according to Error! Reference source not found., are considered and performed. When the stopping condition of the NLS algorithm is reached, the best values of the quadrotor parameters are computed, shown in Table 4. Moreover, the intelligent movement of the parameters during the optimization process for finding the true values is shown in Figure 4. In the first scenario, according to the Figure 5, the quadrotor is able to rotate about only one axis (roll, pitch or yaw axes) to identify  $\Gamma_3$ ,  $\Gamma_6$  and  $\Gamma_8$  parameters. In the second scenario, Figure 6 shows  $\Gamma_2$  and  $\Gamma_5$  parameters are estimated based on the experimental setup, that is free to rotate around its roll and pitch axes. Finally, in the last scenario, according to the Figure 7,  $\Gamma_1$ ,  $\Gamma_4$  and  $\Gamma_7$  parameters of the UAV model are identified by rotate the quadrotor setup around three axis. These results illustrate that the outputs of the simulation results for the quadrotor model are consistent with reality.

Table 3: Scenarios for identification of quadrotor model.

<b>Scenario</b>	<b>Description</b>	<b>Initial Conditions</b>		<b>angular velocity Commands</b>			
I	Roll free	38		2000	2000	2000	3400
	Pitch free	-15		3700	2000	2000	2000
	Yaw free	-75		2000	3300	2000	3300
II	Roll and Pitch free		8 -5	1700	3800	2400	1700
III	Roll, Pitch, and Yaw free	8	-3 -146	1700	3800	2400	1700

Table 4: True values of the quadrotor parameters.

<b>Parameter</b>	<b>Value</b>	<b>Parameter</b>	<b>Value</b>
$\Gamma_1$	-0.9622	$\Gamma_5$	$3.6441 \times 10^{-4}$
$\Gamma_2$	-0.0154	$\Gamma_6$	$7.5395 \times 10^{-5}$
$\Gamma_3$	$5.4716 \times 10^{-5}$	$\Gamma_7$	0.1308
$\Gamma_4$	1.0457	$\Gamma_8$	$4.3753 \times 10^{-5}$

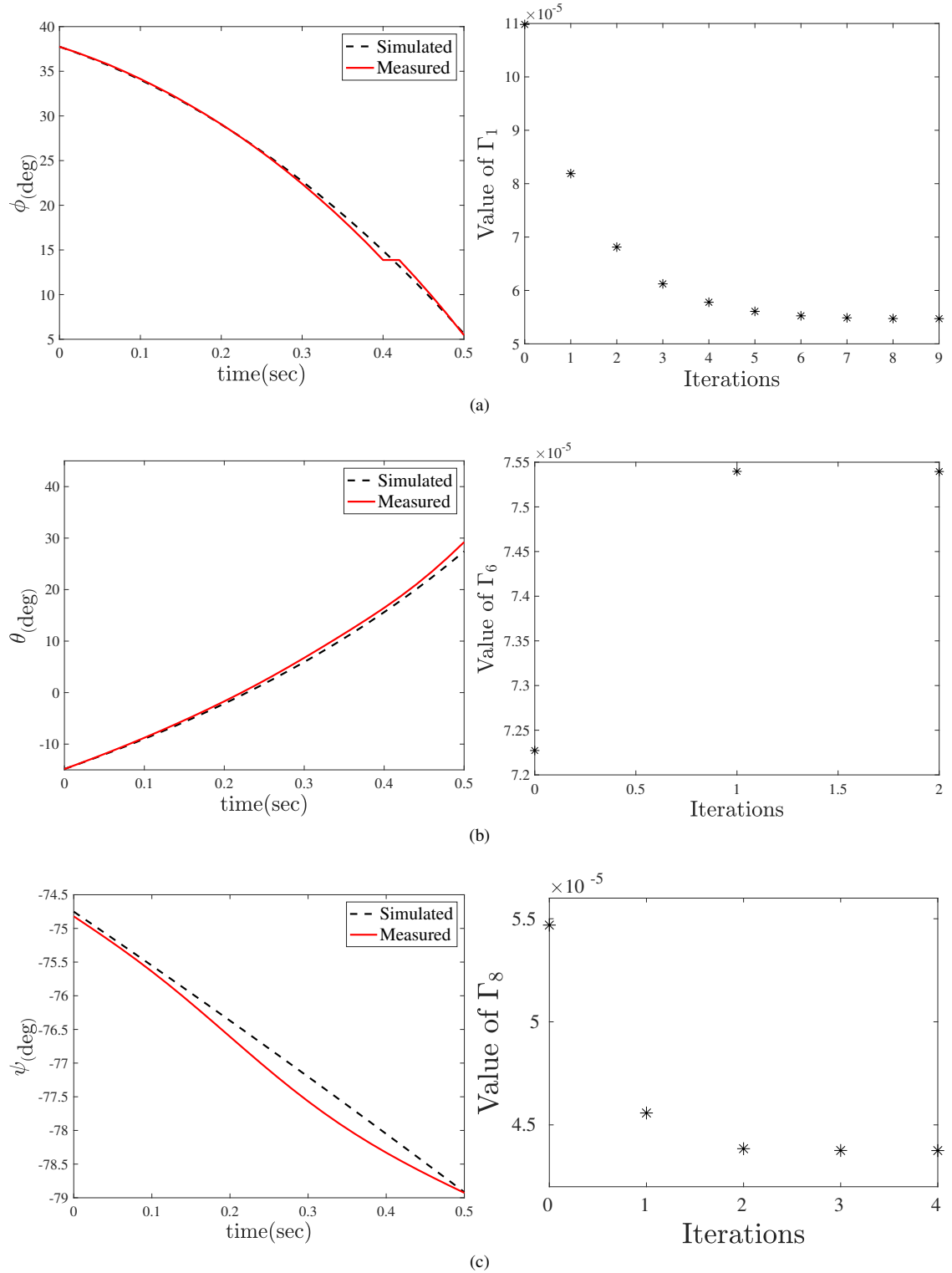


Figure 5: Identification process results when the quadrotor rotates about only one axis: (a) Identification of  $\Gamma_3$  in free roll. (b) Identification of  $\Gamma_6$  in free pitch. (c) Identification of  $\Gamma_8$  in free yaw.

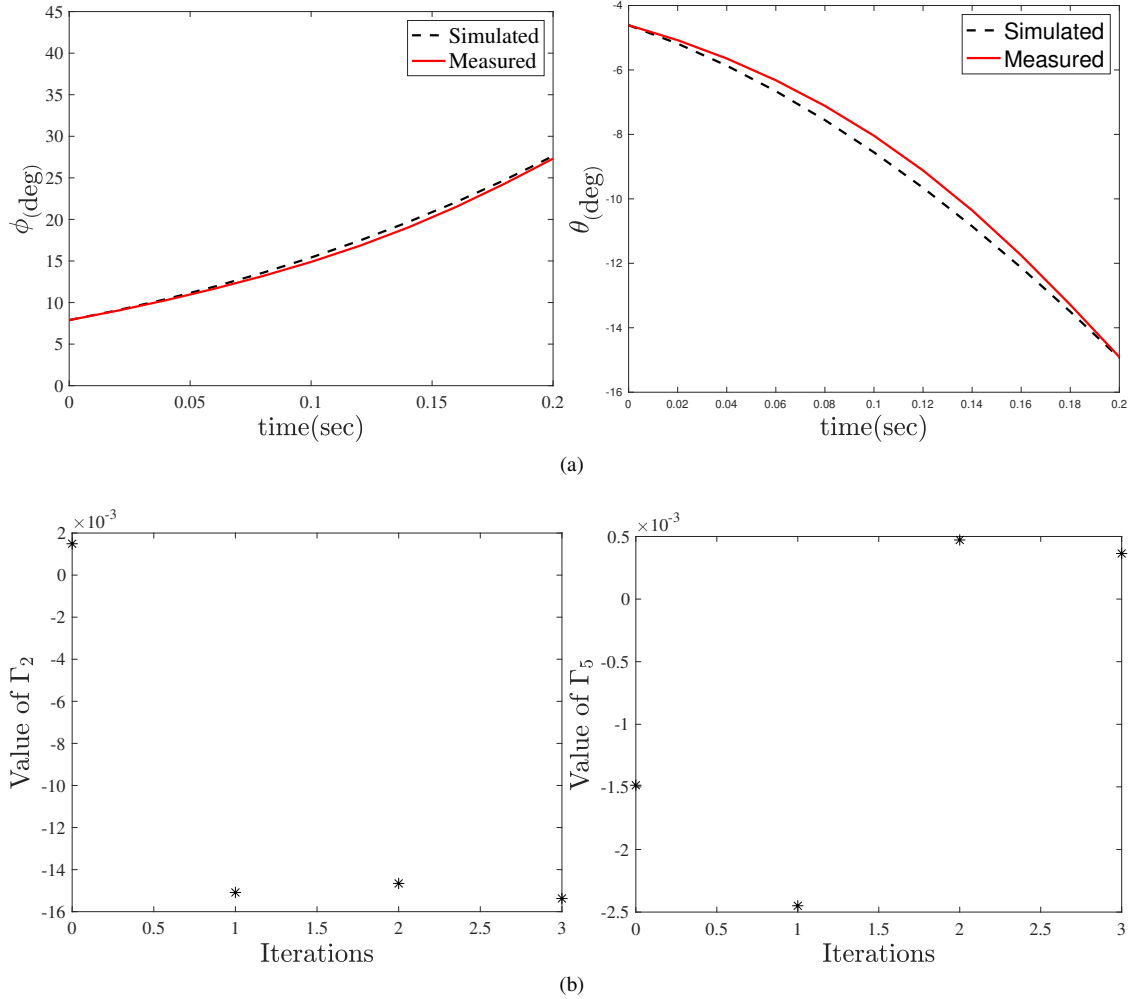


Figure 6: Identification process results when the quadrotor rotates about its roll and pitch axes: (a) Comparison of Simulation and experimental results. (b) Identification of  $\Gamma_2$  and  $\Gamma_5$ .

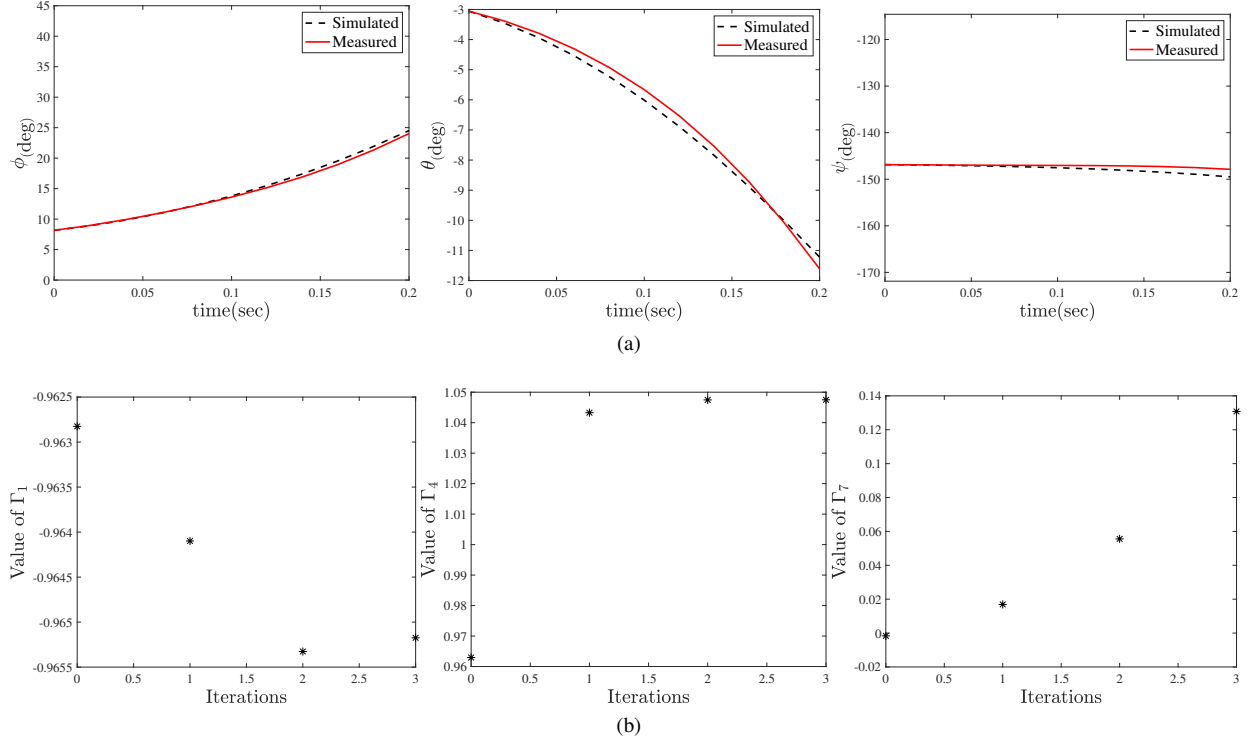


Figure 7: Identification process results when the quadrotor rotates about its roll, pitch, and yaw axes: (a) Comparison of Simulation and experimental results. (b) Identification of  $\Gamma_1$ ,  $\Gamma_4$  and  $\Gamma_7$  parameters.

### 5.2. Performance of the LQIR-DG Controller

Here, the performance of the LQIR-DG controller is evaluated. The desired and actual outputs, including the roll, pitch, and yaw angles, are compared in figure 8. The desired scenario of the simulator is considered a level flight. These figures show that the attitude outputs of the quadrotor converge to the desired values in less than three seconds. Moreover, figure 9 shows the angular velocity command of the quadrotor, respectively. These results illustrate that the LQIR-DG approach appropriately controls the attitude of the experimental setup of the quadrotor.

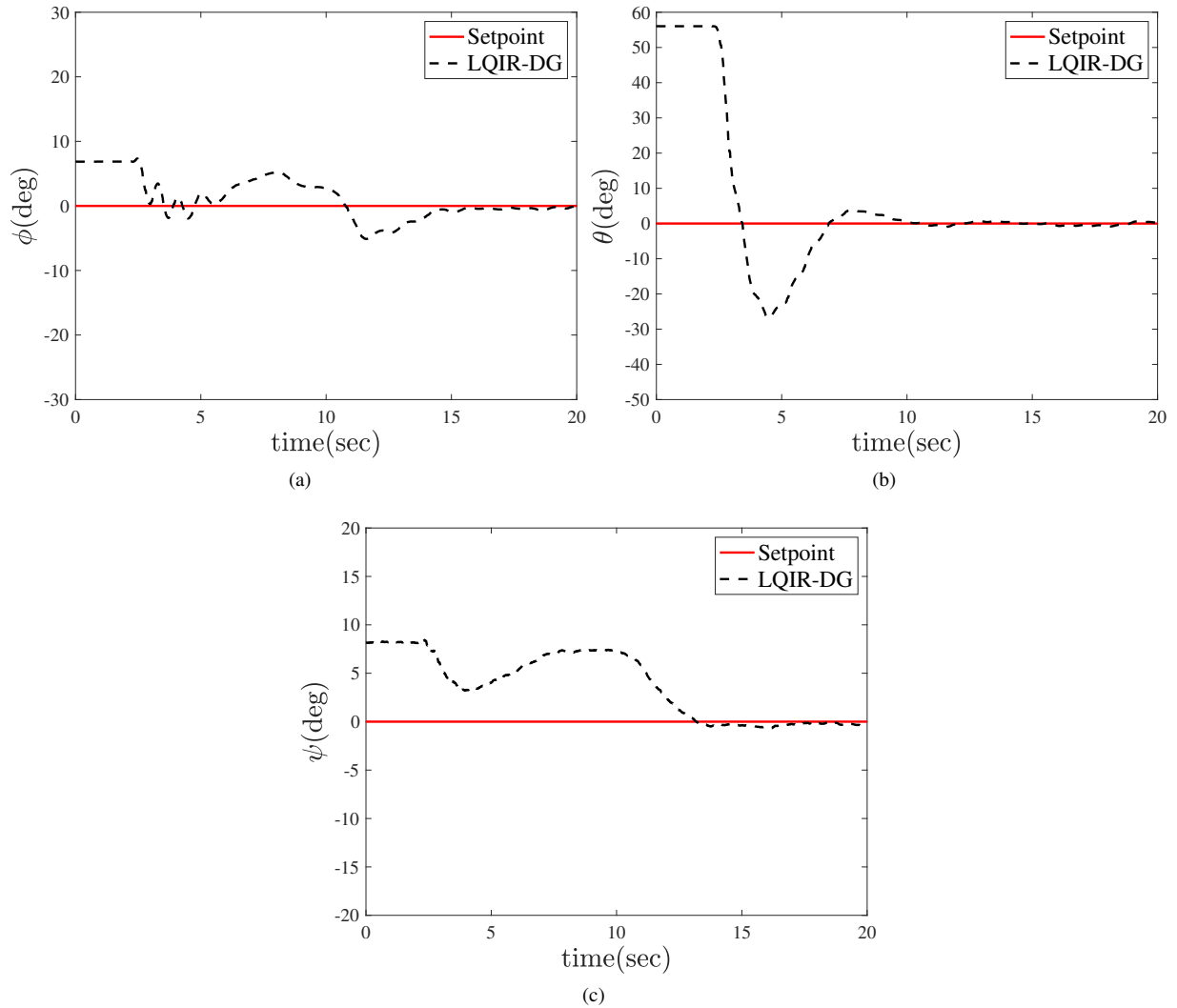


Figure 8: Performance of the LQIR-DG controller (a) roll angle (b) pitch angle (c) yaw angle

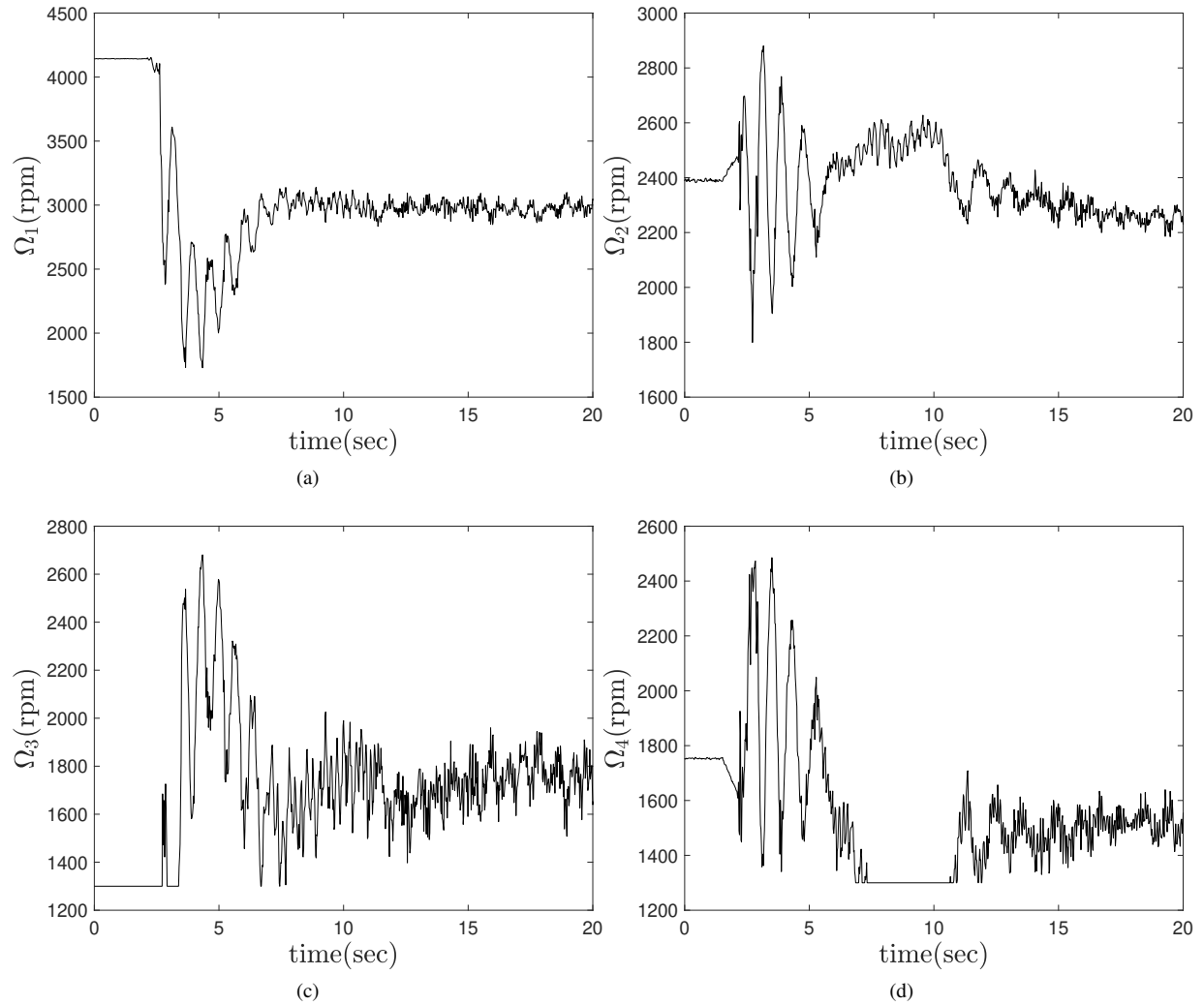


Figure 9: Time history of angular velocity commands

Figure 10 illustrates the performance of the LQIR-DG controller in the coupling mode of the roll and pitch channels to track the desired angle as a square wave with a frequency of 0.02 Hz and an amplitude of 20 degrees.

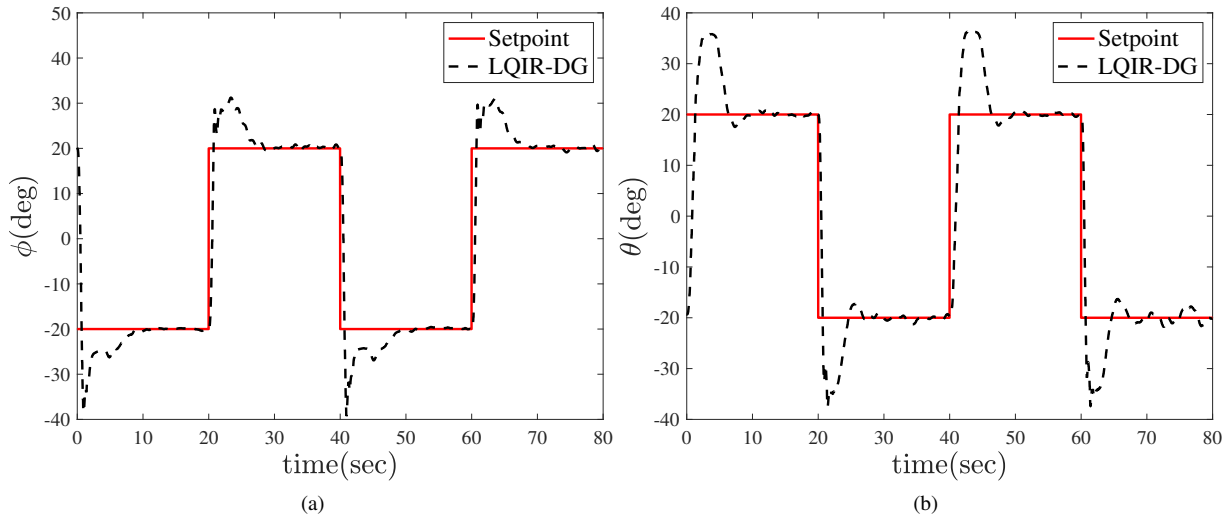


Figure 10: LQIR-DDG controller performance in order to track the desired angles in the two-degree-of-freedom coupling mode (a) Comparison of the roll angle with the desired value (b) Comparison of the pitch angle with the desired

### 5.3. Investigating the possibility of disturbance rejection

This section investigates the possible rejection of input disturbances by the LQIR-DG controller in regulation. For this purpose, a disturbance with an amplitude of 0.5 N is added to the input from 20 to 60 seconds. As shown in figure 11, the LQIR-DG controller performs well in coupling the roll and screw channels to remove the input disturbance. 11 (a), the performance of this controller is checked by comparing the desired roll angle with the actual roll angle. Also, 11 (b) compares the desired pitch angle with the actual pitch angle of the 3DoF experimental setup in removing the input disturbance. The results indicate the proper performance of the controller in removing the input disturbance.

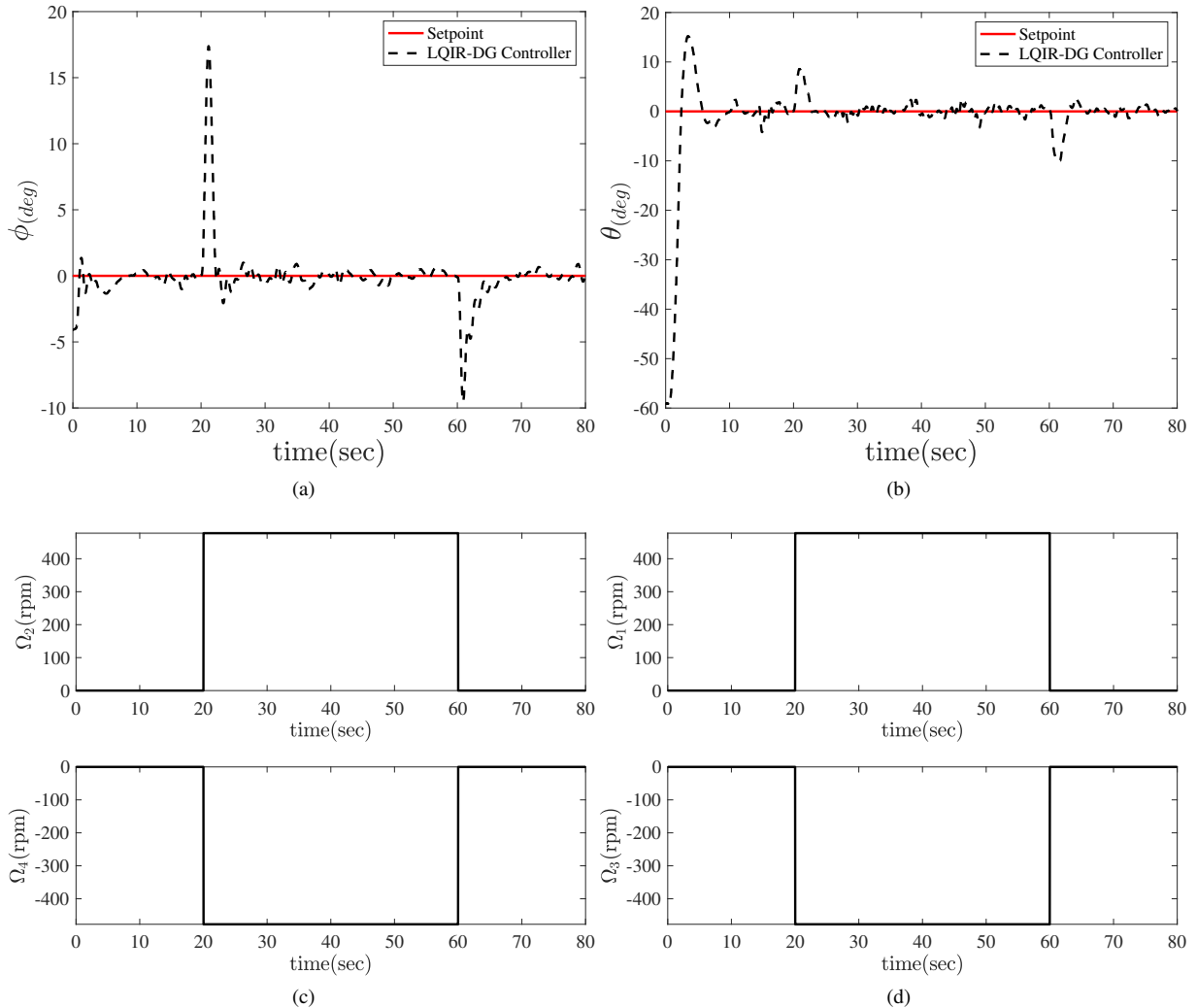


Figure 11: The performance of the LQIR-DG controller in the presence of the input disturbance in the two-degree-of-freedom coupling mode (a) Comparison of the desired roll angle with the actual value (b) Comparison of the desired pitch angle with the actual value.

#### 5.4. Investigating the impact of uncertainty in modeling

This section examines the performance of the LQIR-DG controller designed by considering the uncertainty in 3DoF experimental setup modeling. The performance of the sliding mode controller in the coupling mode of the roll, pitch, and yaw channels is checked by considering the uncertainty in the 3DoF experimental setup modeling in figure 13. For this purpose, 50 grams is added to the roll axis and 100 grams to the pitch axis. In figure 13 (a), the performance of this controller is checked by comparing the desired roll angle with the actual roll angle; In figure 13 (b), the performance of this controller is checked by comparing the desired pitch angle to the actual pitch angle. The implementation results indicate the proper efficiency of the LQIR-DG controller in pursuit of the desired value, taking into account the uncertainty in the values of the moments of inertia around each axis of the body coordinate system.

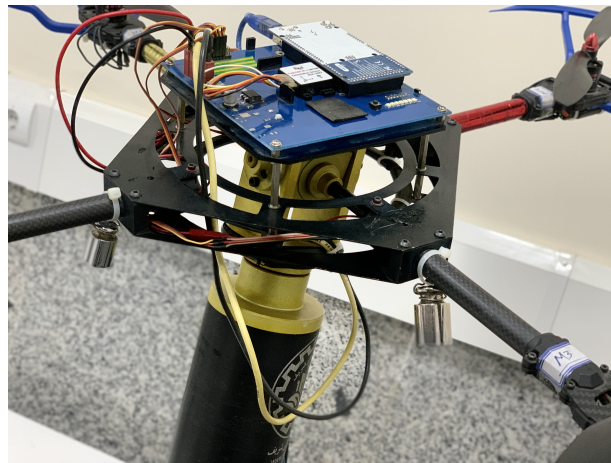


Figure 12: 3DoF setup of the quadrotor with added weight

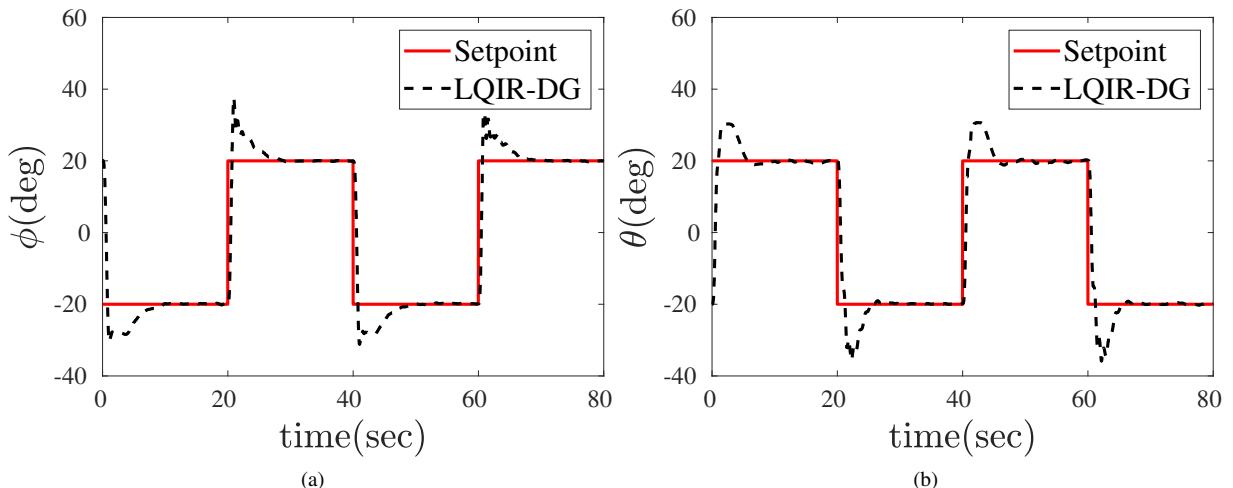


Figure 13: The performance of the LQIR-DG controller by adding weight to each of the roll and pitch axes in the two-degree-of-freedom coupling mode (a) Comparison of the roll angle with the actual value (b) Comparison of the pitch angle with the actual value

### 5.5. Comparison with LQR, LQIR, and PID

Here, the LQIR-DG controller performance is compared with famous control strategies such as the LQR controller method. Figure 14 compares the quadrotor's desired and actual pitch angle in the presence of these controllers. This result indicates that the LQIR-DG controller can provide high tracking performance, such as good transient response and high rapid convergence relative to the LQR controller for pitch angle control of the quadrotor setup.

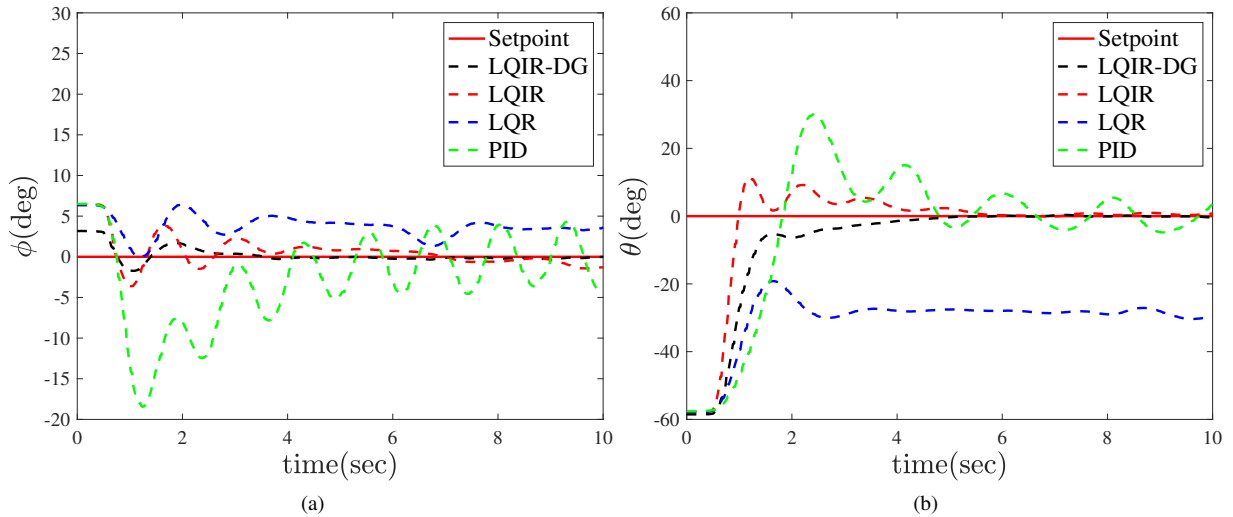


Figure 14: The performance of the LQIR-DG controller by adding weight to each of the roll and pitch axes in the three-degree-of-freedom coupling mode (a) Comparison of the roll angle with the actual value (b) Comparison of the pitch angle with the actual value (c) Comparison of the yaw angle with the actual value

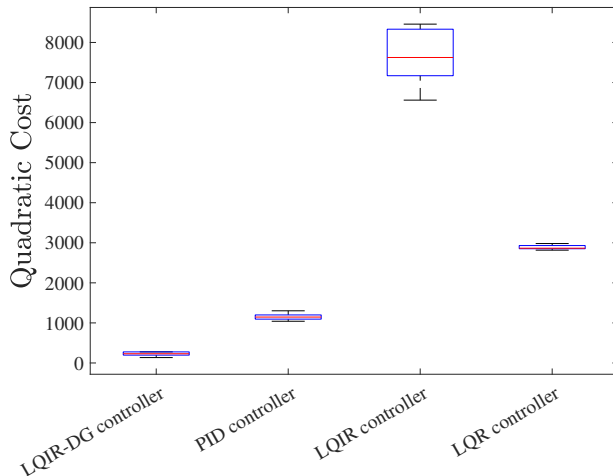


Figure 15: Comparison of the LQIR-DG to the PID quadratic cost function

## 6. Conclusion

In this study, a linear quadratic with integral action based on the differential game theory, called LQIR-DG, was implemented for level attitude control in an experimental setup of a quadrotor. To implement the proposed controller structure, first, an accurate model of the quadrotor was linearized in the state-space form, and then the model parameters were estimated. Next, two players were considered for each of the quadrotor's roll, pitch, and yaw channels. The first player found the best control command for each channel of the setup of a quadrotor based on the mini-maximization of a quadratic criterion; when the second player produced the worst disturbances. Finally, the performance of the proposed controller was investigated in level flight and compared to the LQR controller. The implementation results verify the successful performance of the LQIR-DG method in the level flight of the attitude control for the actual plant.

## References

- [1] M. F. Fathoni, S. Lee, Y. Kim, K.-I. Kim, K. H. Kim, Development of multi-quadrotor simulator based on real-time hypervisor systems, *Drones* 5 (3). doi:10.3390/drones5030059.  
URL <https://www.mdpi.com/2504-446X/5/3/59>
- [2] H. Nobahari, A. Sharifi, A hybridization of extended kalman filter and ant colony optimization for state estimation of nonlinear systems, *Applied Soft Computing* 74. doi:10.1016/j.asoc.2018.10.010.
- [3] H. Bolandi, M. Rezaei, R. Mohsenipour, H. Nemati, S. Smailzadeh, Attitude control of a quadrotor with optimized pid controller, *Intelligent Control and Automation* 04 (2013) 342–349. doi:10.4236/ica.2013.43040.
- [4] A. Abdul Salam, I. Ibraheem, Nonlinear pid controller design for a 6-dof uav quadrotor system, *Engineering Science and Technology, an International Journal* 22. doi:10.1016/j.jestch.2019.02.005.
- [5] Y. Bouzid, M. Zareb, H. Siguerdidjane, M. Guiatni, Boosting a Reference Model-Based Controller Using Active Disturbance Rejection Principle for 3D Trajectory Tracking of Quadrotors: Experimental Validation, *Journal of Intelligent and Robotic Systems* 100 (2) (2020) 597–614. doi:10.1007/s10846-020-01182-4.  
URL <https://hal.univ-grenoble-alpes.fr/hal-02543214>
- [6] Z. Wang, D. Huang, T. Huang, N. Qin, Active disturbance rejection control for a quadrotor uav, in: 2020 IEEE 9th Data Driven Control and Learning Systems Conference (DDCLS), 2020, pp. 1–5. doi:10.1109/DDCLS49620.2020.9275226.
- [7] C. Nicol, C. Macnab, A. Ramirez-Serrano, Robust neural network control of a quadrotor helicopter, in: 2008 Canadian Conference on Electrical and Computer Engineering, 2008, pp. 001233–001238. doi:10.1109/CCECE.2008.4564736.
- [8] L. V. Nguyen, M. D. Phung, Q. P. Ha, Iterative learning sliding mode control for uav trajectory tracking, *Electronics* 10 (20). doi:10.3390/electronics10202474.  
URL <https://www.mdpi.com/2079-9292/10/20/2474>
- [9] K. Liu, R. Wang, S. Dong, X. Wang, Adaptive fuzzy finite-time attitude controller design for quadrotor uav with external disturbances and uncertain dynamics, in: 2022 8th International Conference on Control, Automation and Robotics (ICCAR), 2022, pp. 363–368. doi:10.1109/ICCAR55106.2022.9782598.
- [10] C.-H. Pi, W.-Y. Ye, S. Cheng, Robust quadrotor control through reinforcement learning with disturbance compensation, *Applied Sciences* 11 (7). doi:10.3390/app11073257.  
URL <https://www.mdpi.com/2076-3417/11/7/3257>
- [11] P. Ghiglino, J. L. Forshaw, V. J. Lappas, Online PID Self-Tuning using an Evolutionary Swarm Algorithm with Experimental Quadrotor Flight Results. arXiv:<https://arc.aiaa.org/doi/pdf/10.2514/6.2013-5098>, doi:10.2514/6.2013-5098.  
URL <https://arc.aiaa.org/doi/abs/10.2514/6.2013-5098>
- [12] K. Chara, A. Yassine, F. Srairi, K. Mokhtari, A robust synergetic controller for quadrotor obstacle avoidance using b閦ier curve versus b-spline trajectory generation, *Intelligent Service Robotics* 15. doi:10.1007/s11370-021-00408-0.
- [13] H. Wang, M. Chen, Sliding mode attitude control for a quadrotor micro unmanned aircraft vehicle using disturbance observer, in: Proceedings of 2014 IEEE Chinese Guidance, Navigation and Control Conference, 2014, pp. 568–573. doi:10.1109/CGNCC.2014.7007285.
- [14] A. Aboudonia, A. El-Badawy, R. Rashad, Disturbance observer-based feedback linearization control of an unmanned quadrotor helicopter, *Proceedings of the Institution of Mechanical Engineers Part I Journal of Systems and Control Engineering* 230. doi:10.1177/0959651816656951.
- [15] A. T. Azar, F. E. Serrano, A. Koubaa, N. A. Kamal, Backstepping h-infinity control of unmanned aerial vehicles with time varying disturbances, in: 2020 First International Conference of Smart Systems and Emerging Technologies (SMARTTECH), 2020, pp. 243–248. doi:10.1109/SMArt-TECH49988.2020.00061.
- [16] A. Hamza, A. Mohamed, A. El-Badawy, Robust h-infinity control for a quadrotor uav, 2022. doi:10.2514/6.2022-2033.
- [17] W. Dean, B. Ranganathan, I. Penskiy, S. Bergbreiter, J. Humbert, Robust Gust Rejection on a Micro-air Vehicle Using Bio-inspired Sensing, 2017, pp. 351–362.
- [18] Z. Shulong, A. Honglei, Z. Daibing, S. Lincheng, A new feedback linearization lqr control for attitude of quadrotor, in: 2014 13th International Conference on Control Automation Robotics and Vision (ICARCV), 2014, pp. 1593–1597. doi:10.1109/ICARCV.2014.7064553.
- [19] E. Barzani, K. Salahshoor, A. Khaki Sedigh, Attitude flight control system design of uav using lqg ltr multivariable control with noise and disturbance, in: 2015 3rd RSI International Conference on Robotics and Mechatronics (ICROM), 2015, pp. 188–193. doi:10.1109/ICRoM.2015.7367782.
- [20] J. Engwerda, Linear quadratic games: An overview, Workingpaper, Macroeconomics, subsequently published in *Advances in Dynamic Games and their Applications* (book), 2009 Pagination: 32 (2006).
- [21] J. Engwerda, Min-max robust control in lq-differential games, *Dynamic Games and Applications* 12 (2022) 1–59. doi:10.1007/s13235-021-00421-z.
- [22] Z. Zwierzewicz, On the ship course-keeping control system design by using robust and adaptive control, in: 2014 19th International Conference on Methods and Models in Automation and Robotics (MMAR), 2014, pp. 189–194. doi:10.1109/MMAR.2014.6957349.
- [23] Y. Li, L. Guo, Towards a theory of stochastic adaptive differential games, in: 2011 50th IEEE Conference on Decision and Control and European Control Conference, 2011, pp. 5041–5046. doi:10.1109/CDC.2011.6160768.
- [24] S. Bouabdallah, R. Siegwart, Full control of a quadrotor, in: 2007 IEEE/RSJ International Conference on Intelligent Robots and Systems, 2007, pp. 153–158. doi:10.1109/IROS.2007.4399042.
- [25] S. Bouabdallah, Design and control of quadrotors with application to autonomous flyingdoi:10.5075/epfl-thesis-3727.
- [26] J. Eriksson, Optimization and regularization of nonlinear least squares problems.